

# New Inferences on Magma Dynamics in Melilitite-Carbonatite Volcanoes: The Case Study of Mt. Vulture (Southern Italy)

Gabriele Carnevale<sup>1</sup>, Antonio Caracausi<sup>2</sup>, Silvio Rotolo<sup>3</sup>, Michele Paternoster<sup>4</sup>, and Vittorio Zanon<sup>5</sup>

<sup>1</sup>University of Palermo

<sup>2</sup>Istituto Nazionale di Geofisica e Vulcanologia

<sup>3</sup>Università degli Studi di Palermo, Dipartimento di Scienze della Terra e del Mare, Palermo, Italy

<sup>4</sup>Università della Basilicata

<sup>5</sup>Centro de Vulcanologia e Avaliação de Riscos Geológicos

November 23, 2022

## Abstract

This study provides the first micro-thermometric data of fluid inclusions in mafic loose xenocrysts and ultramafic xenoliths in explosive products of the melilitite-carbonatite Mt. Vulture volcano (southern Italy). We found within ultramafic xenoliths CO<sub>2</sub>-dominated fluid inclusions with trapping pressures between 8.5 and 8.9 kbar, corresponding to a depth of 26-27 km, in proximity of the local crust-mantle boundary. In contrast, trapping pressures within the loose xenocrysts are up to 2.8 and 3.2 kbar (8-9 km). We estimated an ascent rate of the latest 141 ka old melilititic-carbonatitic magmas from the Moho depth to the surface in the range of few hours. Considering the ongoing degassing of mantle-derived CO<sub>2</sub> rich gases at Mt. Vulture, together with geophysical evidences of the presence of low amount of melts at depth, and the tectonic control of the past volcanic activity, our study opens new perspective about the hazardous nature of the “quiescent” melilitite-carbonatite volcanoes.

1 **New Inferences on Magma Dynamics in Melilitite-Carbonatite Volcanoes: The Case**  
2 **Study of Mt. Vulture (Southern Italy)**

3 **G. Carnevale<sup>1</sup>, A. Caracausi<sup>2</sup>, S. G. Rotolo<sup>1,2</sup>, M. Paternoster<sup>2,3</sup>, and V. Zanon<sup>4</sup>**

4 <sup>1</sup> Dipartimento di Scienze della Terra e del Mare, Università degli Studi di Palermo, Palermo,  
5 Italy, <sup>2</sup> Istituto Nazionale di Geofisica e Vulcanologia, Sezione di Palermo, Palermo, Italy, <sup>3</sup>  
6 Dipartimento di Scienze, Università degli Studi della Basilicata, Potenza, Italy, <sup>4</sup> Instituto de  
7 Vulcanologia e Avaliação de Riscos, Universidade dos Açores, Ponta Delgada, Portugal

8 Corresponding author: Gabriele Carnevale ([gabriele.carnevale@unipa.it](mailto:gabriele.carnevale@unipa.it))

9 **Key Points:**

- 10 • Micro-thermometric analyses show the occurrence of high-density CO<sub>2</sub>-rich fluid  
11 inclusions within wehrlite xenoliths
- 12 • Estimates on magma ascent rate show how a melilitite-carbonatite magma can be  
13 comparable with ascent rate of kimberlite magmatism
- 14 • Melilitite-carbonatite volcanoes can be hazardous even after long time of quiescence (>  
15 10<sup>5</sup> years)

## 16 **Abstract**

17 This study provides the first micro-thermometric data of fluid inclusions in mafic loose  
18 xenocrysts and ultramafic xenoliths in explosive products of the melilitite-carbonatite Mt.  
19 Vulture volcano (southern Italy). We found within ultramafic xenoliths CO<sub>2</sub>-dominated fluid  
20 inclusions with trapping pressures between 8.5 and 8.9 kbar, corresponding to a depth of 26-27  
21 km, in proximity of the local crust-mantle boundary. In contrast, trapping pressures within the  
22 loose xenocrysts are up to 2.8 and 3.2 kbar (8-9 km). We estimated an ascent rate of the latest  
23 141 ka old melilititic-carbonatitic magmas from the Moho depth to the surface in the range of  
24 few hours. Considering the ongoing degassing of mantle-derived CO<sub>2</sub> rich gases at Mt. Vulture,  
25 together with geophysical evidences of the presence of low amount of melts at depth, and the  
26 tectonic control of the past volcanic activity, our study opens new perspective about the  
27 hazardous nature of the “quiescent” melilitite-carbonatite volcanoes.

## 28 **Plain Language Summary**

29 The study of fluid inclusions can provide important information about the environments and  
30 magmatological processes in which the host minerals formed. Investigating their composition  
31 and trapping pressure and temperature it is possible to constrain magma ascent history. To  
32 understand the last explosive volcanic activity of Mt. Vulture volcano (southern Italy), we  
33 investigated fluid inclusions in mafic minerals, and ultramafic xenoliths brought to the surface by  
34 a melilitite-carbonatite magma. Our results show the presence of CO<sub>2</sub>-rich fluid inclusions with  
35 trapping pressure corresponding to a depth of 26-27 km in ultramafic xenoliths, and a shallower  
36 depth (8-9 km) in mafic minerals. Estimates on magma ascent rate show rapid ascent dynamics  
37 to the surface (hours). Our study emphasizes the importance of a multidisciplinary approach that  
38 combine geophysics, geochemistry and petrology to investigate a volcanic system even if the  
39 volcano is considered “quiescent”, as is the case of Mt. Vulture volcano, where currently active  
40 magmatic degassing occurs.

## 41 **1 Introduction**

42 Carbonatite magmatism is mainly associated with intraplate continental tectonic settings, with a  
43 temporal distribution from Archean to the present (*e.g.*, Jones et al., 2013; Woolley & Kjarsgaard,  
44 2008), and currently, Oldoinyo Lengai (Tanzania) represents the only active carbonatite volcano,  
45 characterised by a natrocarbonatitic affinity. The growing number of carbonatite occurrences from  
46 unconventional tectonic settings, such as oceanic contexts (*e.g.*, Carnevale et al., 2021; Doucelance  
47 et al., 2010; Mata et al., 2010; Schmidt & Weidendorfer, 2018) or subduction zones (*e.g.*, D’Orazio  
48 et al., 2007; Li et al., 2018), received considerable attention during last two decades, given their  
49 importance as source of rare elements (Verplanck et al., 2019), and, most importantly, because  
50 they provide meaningful information about the geochemical cycle of carbon and mantle  
51 metasomatism as well (*e.g.*, Bouabdellah et al., 2010; Horton, 2021).

52 Mt. Vulture (southern Italy) is an isolated volcano located between the Apulia foreland and the  
53 eastern side of the Apennine orogenic belt, within the particular geodynamic context of the  
54 Apennine subduction zone (D’Orazio et al., 2007; Peccerillo, 2017). This volcano is located along  
55 the deep NE-SW lithospheric faults that represent the tear of the slab, a potential pathway for the

56 ascent of magmatic bodies and mantle derived fluids (Caracausi et al., 2013a; D’Orazio et al.,  
57 2007; Rosenbaum et al., 2008).

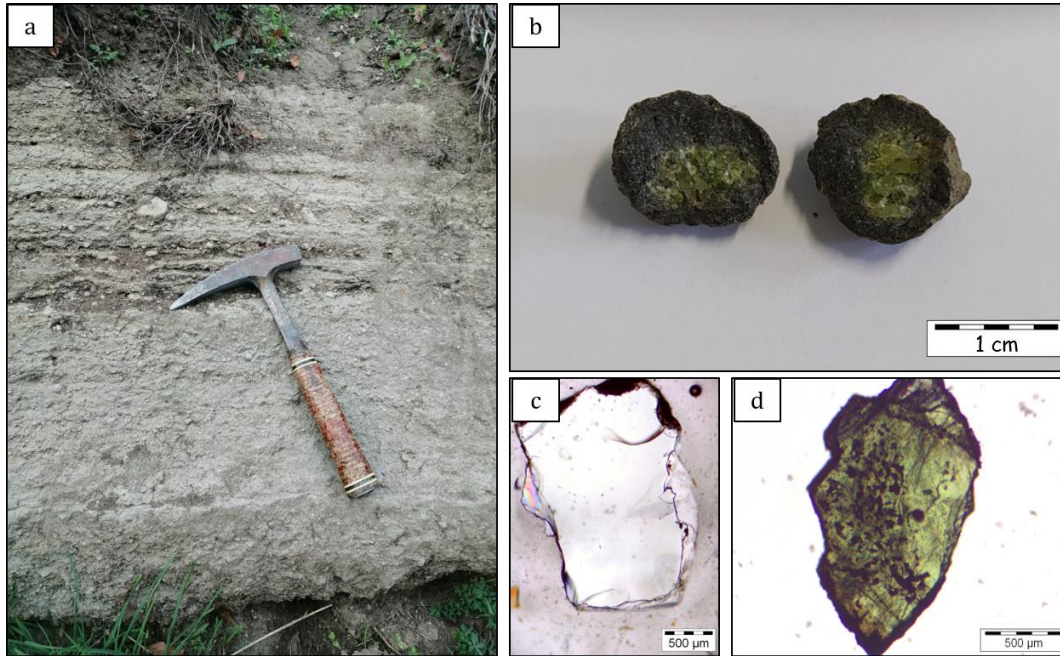
58 The Mt. Vulture volcano is a relatively small volcanic complex characterised by a central vent and  
59 parasitic cones, domes, and lava plugs (Giannandrea et al., 2006). Its eruptive activity started at  
60  $730 \pm 8$  ka (Laurenzi et al., 1993) or  $687 \pm 8$  ka (Villa & Buettner, 2009), and it continued until to  
61  $141 \pm 11$  ka (Villa & Buettner, 2009) with long inter-eruptive periods of quiescence ( $> 10^5$  years,  
62 Buettner et al., 2006). After the initial phase of volcanic activity, represented by pyroclastic  
63 products with lava blocks and subordinate eccentric domes, the latest volcanic event was strongly  
64 explosive, erupting melilitite-carbonatite tephra from maar-type craters (Stoppa & Principe, 1997).  
65 These craters host two lakes (Monticchio Lakes) whose water dissolves mantle-derived volatiles  
66 (Caracausi et al., 2009, 2013b), supporting the active degassing of mantle volatiles from this  
67 volcano (Caracausi et al., 2009, 2015). The last volcanic activity (identified as Monticchio Lakes  
68 Formation, Stoppa & Principe, 1997), fed by a melilitite-carbonatite magma, brought to the surface  
69 some pelletal lapilli (enclosing abundant ultramafic mantle xenoliths and xenocrysts) considered  
70 juvenile component of the melilititic-carbonatitic Monticchio diatreme and volatile component  
71 (Lloyd & Stoppa, 2003). Thus, these products are particularly useful to characterize the mantle  
72 source beneath Mt. Vulture, providing important information about the melilitite-carbonatite  
73 magma and its mantle source.

74 Here we present the first detailed micro-thermometric analysis of fluid inclusions (FIs) hosted in  
75 the ultramafic xenolith cores of pelletal lapilli and in loose olivine and clinopyroxene xenocrysts  
76 from Mt. Vulture volcano (Monticchio Lakes Synthem, Lago Piccolo Sub-Synthem), in order to  
77 describe the way which these very particular magmas are transported to the surface and the  
78 possible implications in terms of volcanic hazard.

## 79 **2 Sample Description**

80 Were selected 29 pelletal lapilli set in a compact fine-grained carbonate-dominated matrix in the  
81 ash-tuff phreatomagmatic deposit of Lago Piccolo Sub-Synthem, with the presence of ultramafic  
82 xenoliths (dominantly wehrlitic) constituting the core of pelletal lapilli, surrounded by a variably  
83 thick rim of micro-phenocrysts (Figures 1a and 1b). We also selected about 200 olivine and 100  
84 emerald-green Cr-diopside loose xenocrysts (Figures 1c and 1d) from the fine-grained carbonate-  
85 rich matrix, where loose xenocrysts of blackish clinopyroxene, amphibole, mica (phlogopite) and  
86 spinel, were also present together with the pelletal lapilli. These loose xenocrysts are considered  
87 as mantle debris from disaggregated nodules. In order to compare the fluid inclusions within the  
88 loose olivine and Cr-diopside xenocrysts with the fluid inclusions within the ultramafic xenolith

89 cores of pelletal lapilli, we selected two representative wehrlite cores from the 29 pelletal lapilli,  
 90 three olivines and two Cr-diopsides from the 200 and 100 loose xenocrysts respectively.



91 **Figure 1.** Sampling site and details on pelletal lapilli and loose crystals. a) Ash-rich tuff surge  
 92 deposit of Lago Piccolo Sub-Synthem. b) Pelletal lapilli with ultramafic xenolith cores. c) Loose  
 93 olivine xenocryst from the fine-grained matrix (parallel polars). d) Loose clinopyroxene (Cr-  
 94 diopside) xenocryst from the fine-grained matrix (parallel polars).

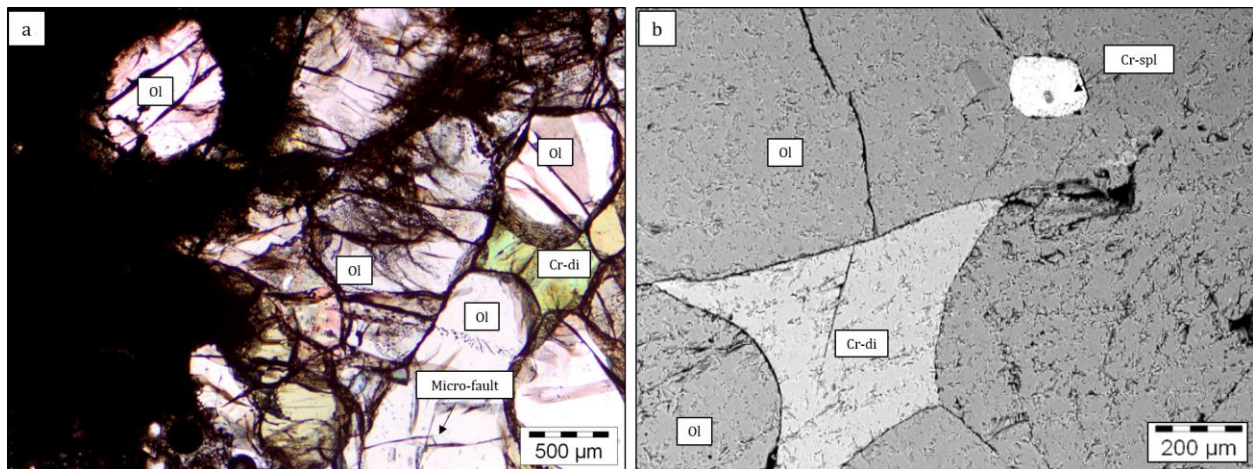
### 95 **3 Results**

96 The ultramafic xenolith cores of pelletal lapilli (the diameter of enclaves vary from 6 to 17 mm)  
 97 are characterised by the presence of Mg-rich olivine ( $F_{090-91}$ , NiO varying from 0.35 to 0.38 wt.  
 98 %, Table S1) and Cr-rich diopside ( $W_{046-48}$ ,  $En_{47-48}$ ,  $Fs_{4-5}$ ) with relatively high  $Cr_2O_3$  content (1.3-  
 99 1.5 wt. %, Table S2). The grain size of the ultramafic xenolith cores is fine- to medium-grained  
 100 (300-600  $\mu m$ ) with equigranular holocrystalline texture, granoblastic or interlocking with  
 101 randomly oriented olivine and clinopyroxene variably elongated (Figures 2a and 2b). The variably  
 102 thick rim of fine-grained material is composed essentially of häuyne micro-phenocrysts, with  
 103 xenocrystic debris of olivine and clinopyroxene (Figure S1).

104 Loose (disaggregated) olivine xenocrysts show very similar composition ( $F_{089-92}$ , NiO = 0.37-0.41  
 105 wt. %, Table S1) if compared with olivine from the ultramafic xenolith cores of pelletal lapilli. In  
 106 the same way, almost all loose clinopyroxene xenocrysts show very similar composition ( $W_{046-48}$ ,  
 107  $En_{47-48}$ ,  $Fs_{4-6}$ ,  $Cr_2O_3$  = 0.4-1.3 wt. %) if compared with clinopyroxene from the ultramafic xenolith  
 108 cores of pelletal lapilli (Table S2). Thus, interestingly, the olivine and Cr-diopside minerals from  
 109 the ultramafic xenoliths (wehrlites) and loose olivine and Cr-diopside xenocrysts, show almost the

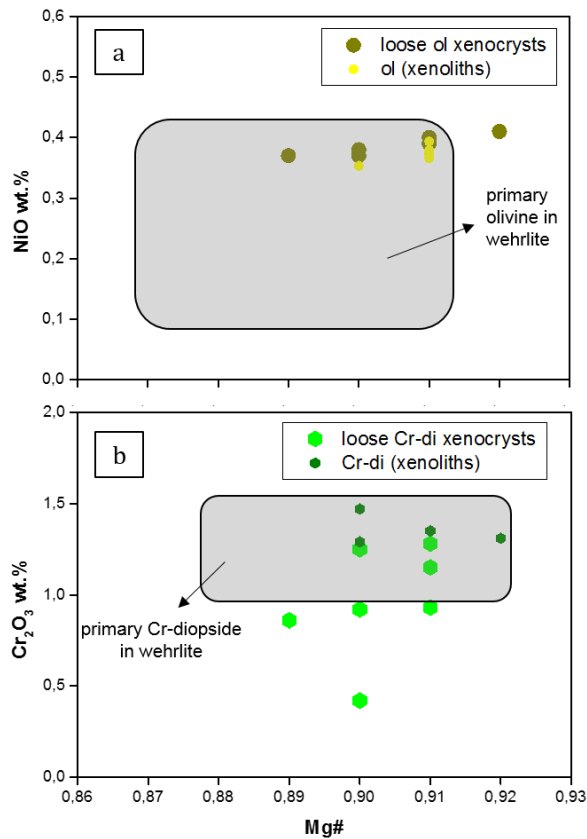
110 same minerochemical composition. Indeed, if plotted onto Mg# vs. NiO wt. % (olivine) and Cr<sub>2</sub>O<sub>3</sub>  
 111 wt. % (Cr-diopside) diagrams, they show narrow ranges (Figures 3a and 3b).

112 All the studied fluid inclusions (FIs) are characterised by pure CO<sub>2</sub>, with melting temperatures  
 113 (T<sub>m</sub>) ranging in a very narrow interval between -56.6 (*i.e.* the triple point of pure CO<sub>2</sub> at 1 bar)  
 114 and -56.8 °C ± 0.1. FIs in loose olivine and Cr-diopside xenocrysts homogenized to liquid phase,  
 115 with temperatures of homogenization (Th) ranging from 11.5 to 30.2 °C ( $\rho = 0.58\text{-}0.85\text{ g/cm}^3$ ) and  
 116 from -20.0 to 13.2 °C ( $\rho = 0.84\text{-}1.03\text{ g/cm}^3$ ), respectively. FIs in the ultramafic cores of lapilli also  
 117 homogenized to liquid phase, at Th ranging from -27.3 to -8.5 °C ( $\rho = 0.98\text{-}1.06\text{ g/cm}^3$ ) in Cr-  
 118 diopside crystals, and from -27.7 to -6.0 °C ( $\rho = 0.96\text{-}1.07\text{ g/cm}^3$ ) in olivine crystals. Data of Th,  
 119 densities, corrected densities and number of measures are reported in Table S3. The main  
 120 geometric measurements of the aspect ratio and the internal structure of pelletal lapilli are reported  
 121 in Table S4. Further details, also about analytical methods, are reported in Supporting Information  
 122 S1.



123 **Figure 2.** Photomicrographs of the ultramafic core of pelletal lapilli from Vulture volcano. a) Sub-  
 124 idioblastic texture with Cr-diopside (emerald green) and elongated olivine crystal with

125 intracrystalline deformations (parallel polars). b) BSE image showing Cr-diopside and olivine  
 126 crystal with Cr-spinel inclusion.



127 **Figure 3.** Minerochemical composition of olivine and Cr-diopside from the ultramafic xenoliths  
 128 (wehrlites) and loose olivine and Cr-diopside xenocrysts from Vulture volcano. a) Mg# vs. NiO  
 129 wt. % in olivine crystals. b) Mg# vs. Cr<sub>2</sub>O<sub>3</sub> wt. % in Cr-diopside crystals. The field of the  
 130 primary olivine and Cr-diopside in wehrlite are from Jones et al. (2000).

#### 131 **4 Significance of Fluid Inclusions Data**

132 In loose olivine and Cr-diopside xenocrysts FIAs are usually rounded or with a slight negative crystal  
 133 shape (Figures 4a and 4b), and in some cases form trails of variable length lined in healed fractures  
 134 (Figure 4c). As regards FIAs in the ultramafic cores of lapilli, they form fluid inclusions assemblages  
 135 (FIAs) (Figure 4d), suggesting single events of entrapment.

136 The histograms of homogenization temperatures (Figure 5a) and densities (Figure 5b) essentially  
 137 show a bimodal distribution, except in some cases where are almost unimodal, depending mainly  
 138 on different trapping events of different products. The highest corrected density values of FIAs are  
 139 in the olivine and Cr-diopside within the ultramafic cores of pelletal lapilli (1.10-1.11 g/cm<sup>3</sup>),  
 140 corresponding to trapping pressures between 8.46 and 8.96 kbar (26-27 km). In the loose Cr-  
 141 diopside xenocrysts trapping events occurred at 8.20-8.65 kbar (25-26 km) and at 6.72-7.22 kbar  
 142 (21-22 km). Conversely, loose olivine xenocrysts show lower density values with a clear density

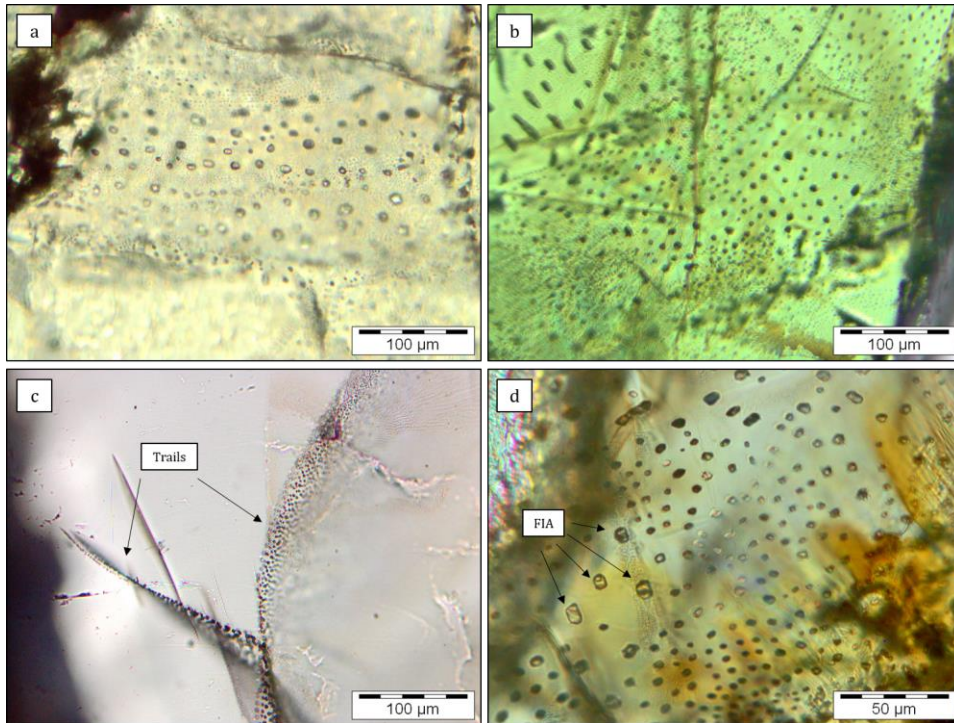
143 peak at  $0.63 \text{ g/cm}^3$  and another at  $0.75 \text{ g/cm}^3$ , with trapping pressures of 2.80-3.12 kbar (8-9 km)  
144 and 4.05-4.49 kbar (12-13 km), respectively. The peak at  $0.63 \text{ g/cm}^3$  is also slightly registered by  
145 olivine within the ultramafic cores.

146 Combining textures, densities and relative distribution of FIs within the ultramafic cores of pelletal  
147 lapilli and loose xenocrysts, it is possible to figure out the different fluid trapping events that  
148 occurred during the transfer of the magmas from crust-mantle boundary to the surface. Olivine and  
149 Cr-diopside within the ultramafic cores of pelletal lapilli, together with loose Cr-diopside  
150 xenocrysts, register the first fluid trapping event at depths corresponding approximately to the  
151 Moho beneath Mt. Vulture (about 32 km, Kelemework et al., 2021). Olivine composition (Fo %,   
152 NiO), clinopyroxene Cr content and spinel Cr/Cr+Al, strongly suggest that the wehrlitic cores are  
153 of mantle origin. Thus, wehrlitic cores of pelletal lapilli are not considered cumulates produced in  
154 shallow level magma chambers and subsequently entrained by the erupting melilitite-carbonatite  
155 magma during ascent to the surface (Beccaluva et al., 2002), but trapping pressures of FIs  
156 constrained the wehrlitic cores of pelletal lapilli to a minimum depth of 26-27 km, near the crust-  
157 mantle boundary. On the contrary, loose olivine xenocrysts record a different fluid trapping event  
158 at much shallower depths, hosting late stage  $\text{CO}_2$ -dominated fluids. It is therefore likely that  
159 olivine and Cr-diopside within the ultramafic xenolith cores of pelletal lapilli and loose Cr-  
160 diopside xenocrysts have different histories of fluid trapping events if compared with loose olivine  
161 xenocrysts, although these latter show very similar minerochemical composition if compared with  
162 olivine within the ultramafic xenolith cores of pelletal lapilli (see Table S1).

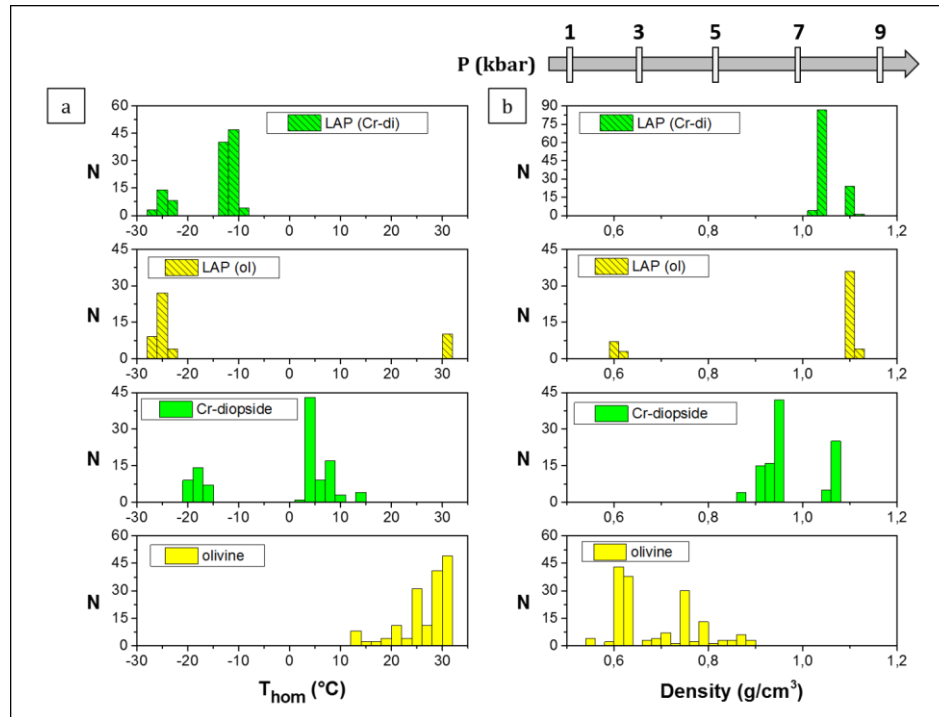
163 A continuous magma ascent translates in a density distribution of FIs with a single frequency  
164 maximum at high-density values, and depending also on parameters such as the ascent velocity,  
165 the original density should be recognizable as the upper limit of measured density values (Hanstee  
166 & Klügel, 2008). On the contrary, if the magma experiences multibaric ponding stages, the density  
167 distribution should show a multi-modal profile (*e.g.*, Zanon et al., 2003). Considering the very low  
168 viscosity of a melilitite-carbonatite magma (*e.g.*, Stagno et al., 2020) and one of the basic  
169 assumptions for the interpretation of FIs (*i.e.* that they have behaved as an isochoric system), it  
170 seems that no fluid re-equilibrating event was registered by studied Mt. Vulture products, simply  
171 showing different histories of fluid trapping events. Thus, we suggest that the melilitite-carbonatite

172 magma transported from Moho depth to the surface the ultramafic mantle xenoliths and Cr-  
 173 diopside loose xenocrysts, while loose olivine xenocrysts were incorporated at shallower depths.

174 It is worthy of note that trapping pressures of volatiles in FIs from loose olivine xenocrysts (2.80-  
 175 4.49 kbar, corresponding to depth of 8-13 km) overlap the depth (6-15 km) of a mafic body within  
 176 the Vulture plumbing system (Improta et al., 2014), suggesting the occurrence of a magma  
 177 stagnation and ponding level before eruption at this depth.



178 **Figure 4.** Thin section photomicrographs (parallel polars) of fluid inclusions and their  
 179 arrangement. FIs within loose a) olivine and b) Cr-diopside xenocrysts. c) Intragranular trails of  
 180 FIs in loose olivine xenocryst. (d) Fluid inclusions assemblage (FIA) in Cr-diopside from the  
 181 ultramafic core of a pelletal lapillus.



182 **Figure 5.** Frequency distribution of a) homogenization temperatures and (b) densities of FIs hosted  
 183 in loose olivine and Cr-diopside xenocrysts and in ultramafic cores of pelletal lapilli from Vulture  
 184 volcano.

### 185 **5 Carbonatite Metasomatism and Magma Ascent Rate**

186 The study of mantle xenoliths represents a great tool to understand the composition and possible  
 187 modification of a mantle source influenced by metasomatic fluids, especially in subduction zones.  
 188 In this framework, the increase of modal clinopyroxene at the expense of orthopyroxene has been  
 189 interpreted as a result of the interaction of ultramafic material with carbonatite melts, and  
 190 carbonatite metasomatism is accompanied by the formation of secondary clinopyroxene formed  
 191 during the reaction of carbonatite melts with orthopyroxene (the melt with the lowest  $\text{SiO}_2$  activity  
 192 dissolves the highest  $\text{SiO}_2$  mantle mineral) (Dalton & Wood, 1993; Russell et al., 2012). Therefore,  
 193 the process of “*wehrlitization*” is considered a consequence of carbonatite metasomatism in the  
 194 lithospheric mantle.

195 Among the Mt. Vulture mantle products, the presence of wehrlite enclaves is widely recognized  
 196 (e.g., Beccaluva et al., 2002; Downes et al., 2002; Jones et al., 2000) and is corroborated by our  
 197 findings where pelletal lapilli cores are largely wehrlitic. Furthermore, according to Zong and Liu,  
 198 (2018), specific crystallochemical patterns in clinopyroxenes (e.g., Mg# vs. Ca/Al; Ca/Al vs.  
 199  $^{87}\text{Sr}/^{86}\text{Sr}$ ) fall into the mantle-related carbonate metasomatism field (Figure S2). Rosatelli et al.  
 200 (2007) also suggest carbonatite melts as the main metasomatism agent of Mt. Vulture mantle  
 201 source region, emphasizing the role of silicate-carbonatite magma immiscibility during the  
 202 carbonated melt ascent to the surface (Solovova et al., 2005), this latter point supported by a  
 203 number of experimental constrains underlying melilititic magma (the last erupted at Mt. Vulture)  
 204 as the best candidate to exsolve an immiscible carbonatite melt (Brooker & Kjarsgaard, 2011).  
 205 Further evidence of metasomatism by carbonatite-like melts is given by the presence of interstitial

206 calcite associated with Fe-Ni-sulfides between olivine grains in a mantle xenolith from Mt. Vulture  
207 (Blanks et al., 2020).

208 Despite the last eruptive event of Mt. Vulture dates back to  $141 \pm 11$  ka (Villa & Buettner, 2009),  
209 geochemical evidences support that active magmatic degassing of mantle-derived volatiles is still  
210 ongoing in Mt. Vulture area (Caracausi et al., 2009, 2013a), also showing how the relationship  
211 between the deep CO<sub>2</sub> release and the time of its last eruption could be an important tool for  
212 evaluating the state of current activity (Caracausi et al., 2015). Moreover, recent studies show how  
213 the source of CO<sub>2</sub> degassing in Mt. Vulture area is related to the presence of a subcontinental  
214 lithospheric mantle (SCLM), that sequesters large amounts of CO<sub>2</sub> due to the infiltration of fluids  
215 and melts during carbonatite-like metasomatism (Bragagni et al., 2022). In this scenario the He  
216 isotopic signature in fluid inclusions of the Vulture mantle xenoliths ( $<6.1R_a$ ;  $R_a$  is the He isotopic  
217 signature in air) overlap the range of the SCLM He end member ( $6.1 \pm 0.9$ ; Gautheron & Moreira,  
218 2002).

219 Considering, 1) the active degassing of mantle-derived fluids in Mt. Vulture area (Caracausi et al.,  
220 2009, 2015), 2) the explosive behaviour associated with a maar-diatreme system of the Monticchio  
221 Lakes Synthem (MLS; Solovova et al., 2005; Stoppa & Principe, 1997), 3) the occurrence of small  
222 amounts of magma at the Moho depth ( $< 1.6$  %, Tumanian et al., 2012), in absence of mantle  
223 upwelling or extensional tectonics that could favour decompression melting (Peccerillo &  
224 Frezzotti, 2015), 4) the role of tectonics in the transfer of the mantle-derived magma and volatiles  
225 and its control of the Vulture volcanism and outgassing (*e.g.*, Caracausi et al., 2013a; D'Orazio et  
226 al., 2007; Rosenbaum et al., 2008), 5) the long inter-eruptive periods ( $> 140$  ka, Buettner et al.,  
227 2006) and 6) the recognized occurring of volatiles rich magmas at the mantle-crust boundary  
228 (Section 4, Significance of Fluid Inclusions Data), we focused on modelling melilitite-carbonatite  
229 magma ascent rate with its cargo of xenoliths and loose xenocrysts to the surface. In order to  
230 constrain the ascent velocity of the melilitite-carbonatite magma, we used the equation from Lister  
231 and Kerr (1991) and applied by Sparks et al. (2006) in their physical model.

232 Taking into consideration (i) a closed system during the magma ascent with a constant dike width  
233 of 1 m, (ii) a magma density of  $2500 \text{ kg/m}^3$ , (iii) a constant viscosity of 0.6 Pa s, and (iv) a mean  
234 density of the crust of  $2600 \text{ kg/m}^3$ , we obtain ascent rate of about 17 m/s (equation (8) from Sparks  
235 et al. 2006), assuming that the buoyancy is the main driving force. Magma viscosity value is taken  
236 from experimental studies of a representative melilitite synthetic melt (Stagno et al., 2020). Magma  
237 density is calculated using the model of Ochs and Lange (1999) at  $1100 \text{ }^\circ\text{C}$  and 10 kbar, assuming  
238 a bulk composition from Stoppa and Principe (1997) with  $\text{SiO}_2 = 37 \text{ wt. } \%$ , and a mean CO<sub>2</sub> value  
239 of 7.5 wt. %, obtained from the H<sub>2</sub>O-CO<sub>2</sub> solubility model proposed by Moussallam et al. (2016).  
240 Indeed, if we consider their model for a low SiO<sub>2</sub>- and H<sub>2</sub>O-free melts (our fluid inclusions study  
241 indicates the presence of pure CO<sub>2</sub> as the main volatile phase, with no presence or very scarce of  
242 H<sub>2</sub>O), at about 30 km depth (crust-mantle boundary beneath Mt. Vulture area), we obtain CO<sub>2</sub>  
243 values between 5 and 10 wt. %. The model of Moussallam et al. (2016) is applied to a kimberlite  
244 magmatism with  $25 \text{ wt. } \% \leq \text{SiO}_2 \leq 32 \text{ wt. } \%$ , and it is comparable to the melilitite-carbonatite  
245 magmatism of Monticchio Lakes Syntheme with  $\text{SiO}_2 < 40 \text{ wt. } \%$  (Stoppa & Principe, 1997).

246 Our result of the ascent rate of the melilitite-carbonatite magma is in the same order of the ascent  
247 rates of kimberlite magmatism described by Moussallam et al. (2016). The direct effect of ascent  
248 dynamics is that the melilitite-carbonatite magma could reach the surface from the depth of 30 km

249 in less than an hour. Considering also recent studies showing how volcanic systems where activity  
250 has remained dormant for protracted periods (> 100 ka) still have the potential for reactivation  
251 (Harangi et al., 2015a; Molnár et al., 2018, 2019), and in Mt. Vulture there is a possible link  
252 between the development of tear faults, magmatism and related magma ascent along these tectonic  
253 pathways (Peccerillo, 2017; Rosenbaum et al., 2008), our study supports that volcanic hazard in  
254 melilitite-carbonatite volcanoes, even after long time of quiescence, should be carefully evaluated.

## 255 **6 Conclusion**

256 We analysed fluid inclusions (FIs) hosted in the wehrlitic cores of pelletal lapilli and in loose  
257 xenocrysts of olivine and clinopyroxene brought to the surface by a melilitite-carbonatite magma  
258 from the last eruption of Mt. Vulture volcano (Monticchio Lakes Synthème, Lago Piccolo Sub-  
259 Synthém). We found CO<sub>2</sub>-dominated FIs with different trapping pressures (from 2.80 to 8.96 kbar)  
260 that correspond to magma storage at different depths within the volcano plumbing system (from 8  
261 to 27 km). The deeper reservoir is close to the local Moho (32 km), while the shallower  
262 corresponds to a solidified magmatic body imaged by geophysical investigations (Improta et al.,  
263 2014). Modeling magma ascent rate results in quite high velocity for melilitite-carbonatite magma  
264 from the crust-mantle boundary to the surface, in the order of 15-20 m/s. These evidences, coupled  
265 to (i) the outgassing of magmatic volatiles at Mt. Vulture, which isotopic signature correspond to  
266 those in the fluid inclusions of the last activity of the volcano (Caracausi et al., 2009, 2013a), and  
267 to (ii) the presence of small amounts of melt (< 1,6%) at the Moho depth, add constraints for  
268 magma production and ascent pathways. Therefore, this study confirms that the scientific  
269 community must pay attention also to the inactive volcanoes, because they could be still hazardous  
270 systems notwithstanding the last volcanic activity occurred hundreds/thousands of years ago.

## 271 **Data Availability Statement**

272 The complete data set of minerochemical and micro-thermometric analyses of this study was  
273 uploaded to the Zenodo FAIR aligned repository ([www.zenodo.org](http://www.zenodo.org)) and will be available for  
274 download at the required link: Carnevale et al. (2022). Micro-thermometry and minerochemical  
275 composition of ultramafic xenoliths and minerals from Mt. Vulture volcano (southern Italy) [Data  
276 set]. Zenodo. <https://doi.org/10.5281/zenodo.6426785>. Accessed 9 april 2022.

## 277 **Acknowledgments**

278 This study was partially funded by Fundação para a Ciência e Tecnologia, Portugal (MAGAT  
279 project, ref. CIRCNA/OCT/0016/2019). The Instituto de Investigação em Vulcanologia e  
280 Avaliação de Riscos (IVAR), Universidade dos Açores, is acknowledged for hosting GC and  
281 providing access to analytical facilities. We are grateful to F. Langone for sampling of some  
282 investigated pelletal lapilli, and to D. Mannetta for his contribution in samples preparation.

## 283 **References**

284 Beccaluva, L., Coltorti, M., Di Girolamo, P., Melluso, L., Milani, L., Morra, V., & Siena, F.  
285 (2002). Petrogenesis and evolution of Mt. Vulture alkaline volcanism (Southern Italy).

- 286 *Mineralogy and Petrology*, 74(2–4), 277–297. <https://doi.org/10.1007/s007100200007>
- 287 Blanks, D. E., Holwell, D. A., Fiorentini, M. L., Moroni, M., Giuliani, A., Tassara, S., et al. (2020).  
288 Fluxing of mantle carbon as a physical agent for metallogenic fertilization of the crust. *Nature*  
289 *Communications*, 11(1). <https://doi.org/10.1038/s41467-020-18157-6>
- 290 Bouabdellah, M., Hoernle, K., Kchit, A., Duggen, S., Hauff, F., Klügel, A., et al. (2010).  
291 Petrogenesis of the Eocene Tamazert continental carbonatites (Central High Atlas, Morocco):  
292 Implications for a common source for the Tamazert and Canary and Cape Verde Island  
293 carbonatites. *Journal of Petrology*, 51, 1655–1686. <https://doi.org/10.1093/petrology/egq033>
- 294 Bragagni, A., Mastroianni, F., Münker, C., Conticelli, S., & Avanzinelli, R. (2022). A carbon-rich  
295 lithospheric mantle as a source for the large CO<sub>2</sub> emissions of Etna volcano (Italy). *Geology*,  
296 50(4), 486–490. <https://doi.org/10.1130/g49510.1>
- 297 Brooker, R. A., & Kjarsgaard, B. A. (2011). Silicate-carbonate liquid immiscibility and phase  
298 relations in the system SiO<sub>2</sub>-Na<sub>2</sub>O-Al<sub>2</sub>O<sub>3</sub>-CaO-CO<sub>2</sub> at 0.1-2.5 GPa with applications to  
299 carbonatite genesis. *Journal of Petrology*, 52, 1281–1305.  
300 <https://doi.org/10.1093/petrology/egq081>
- 301 Buettner, A., Principe, C., Villa, I. M., & Bocchini, D. (2006). Geochronologia <sup>39</sup>Ar-<sup>40</sup>Ar del Monte  
302 Vulture. In C. Principe (Ed.), *La Geologia del Monte Vulture* (pp. 73–86). Lavello.
- 303 Caracausi, A., Nuccio, P. M., Favara, R., Nicolosi, M., & Paternoster, M. (2009). Gas hazard  
304 assessment at the Monticchio crater lakes of Mt. Vulture, a volcano in Southern Italy. *Terra*  
305 *Nova*, 21(2), 83–87. <https://doi.org/10.1111/j.1365-3121.2008.00858.x>
- 306 Caracausi, A., Martelli, M., Nuccio, P. M., Paternoster, M., & Stuart, F. M. (2013a). Active  
307 degassing of mantle-derived fluid: A geochemical study along the Vulture line, southern  
308 Apennines (Italy). *Journal of Volcanology and Geothermal Research*, 253, 65–74.

- 309 <https://doi.org/10.1016/j.jvolgeores.2012.12.005>
- 310 Caracausi, A., Nicolosi, M., Nuccio, P. M., Favara, R., Paternoster, M., & Rosciglione, A. (2013b).  
311 Geochemical insight into differences in the physical structures and dynamics of two adjacent  
312 maar lakes at Mt. Vulture volcano (southern Italy). *Geochemistry, Geophysics, Geosystems*,  
313 *14*(5), 1411–1434. <https://doi.org/10.1002/ggge.20111>
- 314 Caracausi, A., Paternoster, M., & Nuccio, P. M. (2015). Mantle CO<sub>2</sub> degassing at Mt. Vulture  
315 volcano (Italy): Relationship between CO<sub>2</sub> outgassing of volcanoes and the time of their last  
316 eruption. *Earth and Planetary Science Letters*, *411*, 268–280.  
317 <https://doi.org/10.1016/j.epsl.2014.11.049>
- 318 Carnevale, G., Caracausi, A., Correale, A., Italiano, L., & Rotolo, S. G. (2021). An overview of  
319 the geochemical characteristics of oceanic carbonatites: New insights from fuerteventura  
320 carbonatites (Canary islands). *Minerals*, *11*(2). <https://doi.org/10.3390/min11020203>
- 321 Carnevale, G., Caracausi, A., Rotolo, S. G., Paternoster, M., & Zanon, V. (2022). Micro-  
322 thermometry and minerochemical composition of ultramafic xenoliths and minerals from Mt.  
323 Vulture volcano (southern Italy) [Data set]. Zenodo. <https://doi.org/10.5281/zenodo.6426785>
- 324 D’Orazio, M., Innocenti, F., Tonarini, S., & Doglioni, C. (2007). Carbonatites in a subduction  
325 system: The Pleistocene alvikites from Mt. Vulture (southern Italy). *Lithos*, *98*(1–4), 313–  
326 334. <https://doi.org/10.1016/j.lithos.2007.05.004>
- 327 Dalton, J. A., & Wood, B. J. (1993). The compositions of primary carbonate melts and their  
328 evolution through wallrock reaction in the mantle. *Earth and Planetary Science Letters*, *119*,  
329 511–525. [https://doi.org/10.1016/0012-821X\(93\)90059-I](https://doi.org/10.1016/0012-821X(93)90059-I)
- 330 Doucelance, R., Hammouda, T., Moreira, M., & Martins, J. C. (2010). Geochemical constraints  
331 on depth of origin of oceanic carbonatites: The Cape Verde case. *Geochimica et*

- 332 *Cosmochimica Acta*, 74, 7261–7282. <https://doi.org/10.1016/j.gca.2010.09.024>
- 333 Downes, H., Kostoula, T., Jones, A. P., Beard, A. D., Thirlwall, M. F., & Bodinier, J. L. (2002).  
334 Geochemistry and Sr-Nd isotopic compositions of mantle xenoliths from the Monte Vulture  
335 carbonatite-melilitite volcano, central southern Italy. *Contributions to Mineralogy and*  
336 *Petrology*, 144(1), 78–92. <https://doi.org/10.1007/s00410-002-0383-4>
- 337 Gautheron, C., & Moreira, M. (2002). Helium signature of the subcontinental lithospheric mantle.  
338 *Earth and Planetary Science Letters*, 199, 39–47. [https://doi.org/10.1016/S0012-](https://doi.org/10.1016/S0012-821X(02)00563-0)  
339 [821X\(02\)00563-0](https://doi.org/10.1016/S0012-821X(02)00563-0)
- 340 Giannandrea, P., La Volpe, L., Principe, C., & Schiattarella, M. (2006). Unità stratigrafiche a limiti  
341 inconformi e storia evolutiva del vulcano medio-pleistocenico di Monte Vulture (Appennino  
342 meridionale, Italia). *Bollettino Della Societa Geologica Italiana*, 125(1), 67–92.
- 343 Hansteen, T. H., & Klügel, A. (2008). Fluid inclusion thermobarometry as a tracer for magmatic  
344 processes. *Reviews in Mineralogy and Geochemistry*, 69(Roedder 1984), 143–177.  
345 <https://doi.org/10.2138/rmg.2008.69.5>
- 346 Harangi, S., Lukács, R., Schmitt, A. K., Dunkl, I., Molnár, K., Kiss, B., et al. (2015). Constraints  
347 on the timing of Quaternary volcanism and duration of magma residence at Ciomadul  
348 volcano, east-central Europe, from combined U-Th/He and U-Th zircon geochronology.  
349 *Journal of Volcanology and Geothermal Research*, 301, 66–80.  
350 <https://doi.org/10.1016/j.jvolgeores.2015.05.002>
- 351 Horton, F. (2021). Rapid recycling of subducted sedimentary carbon revealed by Afghanistan  
352 carbonatite volcano. *Nature Geoscience*, 14(7), 508–512. [https://doi.org/10.1038/s41561-](https://doi.org/10.1038/s41561-021-00764-7)  
353 [021-00764-7](https://doi.org/10.1038/s41561-021-00764-7)
- 354 Improta, L., De Gori, P., & Chiarabba, C. (2014). New insights into crustal structure, Cenozoic

- 355 magmatism, CO<sub>2</sub> degassing, and seismogenesis in the southern Apennines and Irpinia region  
356 from local earthquake tomography. *Journal of Geophysical Research: Solid Earth*, 119(11),  
357 8283–8311. <https://doi.org/10.1002/2013JB010890>
- 358 Jones, A. P., Kostoula, T., Stoppa, F., & Woolley, A. R. (2000). Petrography and mineral chemistry  
359 of mantle xenoliths in a carbonate-rich melilititic tuff from Mt. Vulture volcano, southern  
360 Italy. *Mineralogical Magazine*, 64(4), 593–613. <https://doi.org/10.1180/002646100549634>
- 361 Jones, A. P., Genge, M., & Carmody, L. (2013). Carbonate melts and carbonatites. *Reviews in*  
362 *Mineralogy and Geochemistry*, 75, 289–322. <https://doi.org/10.2138/rmg.2013.75.10>
- 363 Kelemework, Y., Milano, M., La Manna, M., de Alteriis, G., Iorio, M., & Fedi, M. (2021). Crustal  
364 structure in the Campanian region (Southern Apennines, Italy) from potential field modelling.  
365 *Scientific Reports*, 11(1), 1–18. <https://doi.org/10.1038/s41598-021-93945-8>
- 366 Laurenzi, M.A., Brocchini, D., Principe, C., & Ferrara, G. (1993). Mt. Vulture volcano  
367 chronostratigraphy and the effectiveness of dating young phlogopites. Abstracts EUG 7,  
368 Strasburgo, 572-573.
- 369 Li, Y., Zhang, J., Mostofa, K. M. G., Wang, Y., Yu, S., Cai, Z., et al. (2018). Petrogenesis of  
370 carbonatites in the Luliangshan region, North Qaidam, northern Tibet, China: Evidence for  
371 recycling of sedimentary carbonate and mantle metasomatism within a subduction zone.  
372 *Lithos*, 322, 148–165. <https://doi.org/10.1016/j.lithos.2018.10.010>
- 373 Lister, J. R., & Kerr, R. C. (1991). Fluid-mechanical models of crack propagation and their  
374 application to magma transport in dykes. *Journal of Geophysical Research*, 96(B6), 49–77.  
375 <https://doi.org/10.1029/91jb00600>
- 376 Lloyd, F. E., & Stoppa, F. (2003). Pelletal Lapilli in Diatremes – Some Inspiration from the Old  
377 Masters. *GeoLines*, 15, 65–71.

- 378 Mata, J., Moreira, M., Doucelance, R., Ader, M., & Silva, L. C. (2010). Noble gas and carbon  
379 isotopic signatures of Cape Verde oceanic carbonatites: Implications for carbon provenance.  
380 *Earth and Planetary Science Letters*, 291, 70–83. <https://doi.org/10.1016/j.epsl.2009.12.052>
- 381 Molnár, K., Harangi, S., Lukács, R., Dunkl, I., Schmitt, A. K., Kiss, B., et al. (2018). The onset of  
382 the volcanism in the Ciomadul Volcanic Dome Complex (Eastern Carpathians): Eruption  
383 chronology and magma type variation. *Journal of Volcanology and Geothermal Research*,  
384 354, 39–56. <https://doi.org/10.1016/j.jvolgeores.2018.01.025>
- 385 Molnár, K., Lukács, R., Dunkl, I., Schmitt, A. K., Kiss, B., Seghedi, I., et al. (2019). Episodes of  
386 dormancy and eruption of the Late Pleistocene Ciomadul volcanic complex (Eastern  
387 Carpathians, Romania) constrained by zircon geochronology. *Journal of Volcanology and*  
388 *Geothermal Research*, 373, 133–147. <https://doi.org/10.1016/j.jvolgeores.2019.01.025>
- 389 Moussallam, Y., Morizet, Y., & Gaillard, F. (2016). H<sub>2</sub>O–CO<sub>2</sub> solubility in low SiO<sub>2</sub>-melts and  
390 the unique mode of kimberlite degassing and emplacement. *Earth and Planetary Science*  
391 *Letters*, 447, 151–160. <https://doi.org/10.1016/j.epsl.2016.04.037>
- 392 Ochs, F. A., & Lange, R. A. (1999). The density of hydrous magmatic liquids. *Science*, 283(5406),  
393 1314–1317. <https://doi.org/10.1126/science.283.5406.1314>
- 394 Peccerillo, A., & Frezzotti, M. L. (2015). Magmatism, mantle evolution and geodynamics at the  
395 converging plate margins of Italy. *Journal of the Geological Society*, 172(4), 407–427.  
396 <https://doi.org/10.1144/jgs2014-085>
- 397 Peccerillo, A. (2017). The Apulian Province (Mount Vulture). *Advances in Volcanology*, 203–  
398 216. [https://doi.org/10.1007/978-3-319-42491-0\\_8](https://doi.org/10.1007/978-3-319-42491-0_8)
- 399 Rosatelli, G., Wall, F., & Stoppa, F. (2007). Calcio-carbonatite melts and metasomatism in the  
400 mantle beneath Mt. Vulture (Southern Italy). *Lithos*, 99(3–4), 229–248.

- 401 <https://doi.org/10.1016/j.lithos.2007.05.011>
- 402 Rosenbaum, G., Gasparon, M., Lucente, F. P., Peccerillo, A., & Miller, M. S. (2008). Kinematics  
403 of slab tear faults during subduction segmentation and implications for Italian magmatism.  
404 *Tectonics*, 27(2), 1–16. <https://doi.org/10.1029/2007TC002143>
- 405 Russell, J. K., Porritt, L. A., Lavallé, Y., & Dingwell, D. B. (2012). Kimberlite ascent by  
406 assimilation-fuelled buoyancy. *Nature*, 481(7381), 352–356.  
407 <https://doi.org/10.1038/nature10740>
- 408 Schmidt, M. W., & Weidendorfer, D. (2018). Carbonatites in oceanic hotspots. *Geology*, 46, 435–  
409 438. <https://doi.org/10.1130/G39621.1>
- 410 Solovova, I. P., Girnis, A. V., Kogarko, L. N., Kononkova, N. N., Stoppa, F., & Rosatelli, G.  
411 (2005). Compositions of magmas and carbonate-silicate liquid immiscibility in the Vulture  
412 alkaline igneous complex, Italy. *Lithos*, 85(1-4 SPEC. ISS.), 113–128.  
413 <https://doi.org/10.1016/j.lithos.2005.03.022>
- 414 Sparks, R. S. J., Baker, L., Brown, R. J., Field, M., Schumacher, J., Stripp, G., & Walters, A.  
415 (2006). Dynamical constraints on kimberlite volcanism. *Journal of Volcanology and*  
416 *Geothermal Research*, 155(1–2), 18–48. <https://doi.org/10.1016/j.jvolgeores.2006.02.010>
- 417 Stagno, V., Stopponi, V., Kono, Y., D’arco, A., Lupi, S., Romano, C., et al. (2020). The viscosity  
418 and atomic structure of volatile-bearing melilititic melts at high pressure and temperature and  
419 the transport of deep carbon. *Minerals*, 10(3), 1–13. <https://doi.org/10.3390/min10030267>
- 420 Stoppa, F., & Principe, C. (1997). Eruption style and petrology of a new carbonatitic suite from  
421 the Mt. Vulture Southern Italy /: The Monticchio Lakes Formation. *Journal of Volcanology*  
422 *and Geothermal Research*, 78(3–4), 251–265. [https://doi.org/10.1016/S0377-](https://doi.org/10.1016/S0377-0273(97)00004-8)  
423 [0273\(97\)00004-8](https://doi.org/10.1016/S0377-0273(97)00004-8)

- 424 Tumanian, M., Frezzotti, M. L., Peccerillo, A., Brandmayr, E., & Panza, G. F. (2012). Thermal  
425 structure of the shallow upper mantle beneath Italy and neighbouring areas: Correlation with  
426 magmatic activity and geodynamic significance. *Earth-Science Reviews*, *114*(3–4), 369–385.  
427 <https://doi.org/10.1016/j.earscirev.2012.07.002>
- 428 Verplanck, P. L., Mariano, A. N., & Mariano, A. (2019). Rare Earth Element Ore Geology of  
429 Carbonatites. *Rare Earth and Critical Elements in Ore Deposits*, 5–32.  
430 <https://doi.org/10.5382/rev.18.01>
- 431 Villa, I. M., & Buettner, A. (2009). Chronostratigraphy of Monte Vulture volcano (southern Italy):  
432 Secondary mineral microtextures and  $^{39}\text{Ar}$ - $^{40}\text{Ar}$  systematics. *Bulletin of Volcanology*, *71*(10),  
433 1195–1208. <https://doi.org/10.1007/s00445-009-0294-6>
- 434 Woolley, A. R., & Kjarsgaard, B. A. (2008). Carbonatite occurrences of the world: map and  
435 database. *Geological Survey of Canada*, *5796*, 1–28.  
436 <https://doi.org/https://doi.org/10.4095/225115>
- 437 Zanon, V., Frezzotti, M.-L., & Peccerillo, A. (2003). Magmatic feeding system and crustal magma  
438 accumulation beneath Vulcano Island (Italy): Evidence from  $\text{CO}_2$  fluid inclusions in quartz  
439 xenoliths . *Journal of Geophysical Research: Solid Earth*, *108*(B6).  
440 <https://doi.org/10.1029/2002jb002140>
- 441 Zong, K., & Liu, Y. (2018). Carbonate metasomatism in the lithospheric mantle: Implications for  
442 cratonic destruction in North China. *Science China Earth Sciences*, *61*(6), 711–729.  
443 <https://doi.org/10.1007/s11430-017-9185-2>

444 **References From the Supporting Information**

- 445 Bakker, R. J. (2003). Package FLUIDS 1. Computer programs for analysis of fluid inclusion data  
446 and for modelling bulk fluid properties. *Chemical Geology*, 194(1–3), 3–23.  
447 [https://doi.org/10.1016/S0009-2541\(02\)00268-1](https://doi.org/10.1016/S0009-2541(02)00268-1)
- 448 D’Orazio, M., Innocenti, F., Tonarini, S., & Doglioni, C. (2008). Reply to the discussion of:  
449 “Carbonatites in a subduction system: The Pleistocene alvikites from Mt. Vulture (Southern  
450 Italy)” by M. D’Orazio, F. Innocenti, S. Tonarini and C. Doglioni (*Lithos* 98, 313-334) by F.  
451 Stoppa, C. Principe and P. Giannandrea. *Lithos*, 103(3–4), 557–561.  
452 <https://doi.org/10.1016/j.lithos.2007.10.010>
- 453 Gernon, T. M., Brown, R. J., Tait, M. A., & Hincks, T. K. (2012). The origin of pelletal lapilli in  
454 explosive kimberlite eruptions. *Nature Communications*, 3, 832–837.  
455 <https://doi.org/10.1038/ncomms1842>
- 456 Scrocca, D., Sciamanna, S., Di Luzio, E., Tozzi, M., Nicolai, C., & Gambini, R. (2007). Structural  
457 setting along the CROP-04 deep seismic profile (Southern Apennines - Italy). *Bollettino*  
458 *Della Società Geologica Italiana*, Supplemento, 7, 283–296.
- 459 Sterner, S. M., & Bodnar, R. J. (1991). Synthetic fluid inclusions. X: Experimental determination  
460 of P-V-T-X properties in the CO<sub>2</sub>-H<sub>2</sub>O system to 6 kb and 700 °C. *American Journal of*  
461 *Science*, 291, 1–54. <https://doi.org/https://doi.org/10.2475/ajs.291.1.1>
- 462 Stoppa, F., Principe, C., & Giannandrea, P. (2008). Comments on: Carbonatites in a subduction  
463 system: The Pleistocene alvikites from Mt. Vulture (southern Italy) by d’Orazio et al., (2007).  
464 *Lithos*, 103(3–4), 550–556. <https://doi.org/10.1016/j.lithos.2007.10.012>

**New Inferences on Magma Dynamics in Melilitite-Carbonatite Volcanoes: The Case Study of Mt. Vulture (Southern Italy)**

G. Carnevale<sup>1</sup>, A. Caracausi<sup>2</sup>, S. G. Rotolo<sup>1,2</sup>, M. Paternoster<sup>3</sup>, and V. Zanon<sup>4</sup>

<sup>1</sup> Dipartimento di Scienze della Terra e del Mare, Università degli Studi di Palermo, Palermo, Italy, <sup>2</sup> Istituto Nazionale di Geofisica e Vulcanologia, Sezione di Palermo, Palermo, Italy, <sup>3</sup> Dipartimento di Scienze, Università degli Studi della Basilicata, Potenza, Italy, <sup>4</sup> Instituto de Vulcanologia e Avaliação de Riscos, Universidade dos Açores, Ponta Delgada, Portugal

**Contents of this file**

Text S1 (Geological Background, Petrography and Mineral Chemistry, Fluid Inclusions, Analytical Methods, Geometric Parameters of Pelletal Lapilli)  
Figures S1 to S3  
Tables S1 to S4

**Introduction**

This supplementary information file includes a general description of the geological background of the Mt. Vulture and further details about petrography, mineral chemistry and fluid inclusions of the study samples, with also details about analytical methods and geometries of the pelletal lapilli. Figure [S1](#) shows the core and the fine-grained mineral assemblage of the rim of the pelletal lapilli. Figure [S2](#) shows diagrams of some geochemical tracers from Mt. Vulture loose clinopyroxene xenocrysts. Figure [S3](#) shows diagrams of the main geometric characteristics of pelletal lapilli. Table [S1](#) shows minerochemical composition of olivine from the core of pelletal lapilli and loose olivine xenocrysts. Table [S2](#) shows minerochemical composition of clinopyroxene from the core of pelletal lapilli and loose clinopyroxene xenocrysts. Table [S3](#) shows the microthermometric data. Table [S4](#) shows the geometric parameters of pelletal lapilli.

## **Text S1.**

### **Geological Background.**

Mount Vulture is one of the major Quaternary volcanoes of the central Italian peninsula, located within Apulian foreland with a consistent east offset with respect to the peri-thyrrhenian Campanian-Latium-Tuscany volcanic alignment. The Moho beneath the Mt. Vulture is around 32 km with a lithospheric thickness approaching 100 km (Kelemework et al., 2021; Peccerillo, 2017). Mt. Vulture volcano activity started at ca. 740 ka and continued until ca. 480 ka (Villa & Buettner, 2009). After a long period of quiescence, a small volume explosive eruption of carbonatite-melilitite magma at about 140 ka (Villa & Buettner, 2009) occurred, forming also two intra-caldera maars, now occupied by the Monticchio Lakes (D'Orazio et al., 2007; Stoppa & Principe, 1997).

The erupted silicate magmas are all silica undersaturated, ranging from foidites (leucitites, haünites, nephelinites), tephrites and basanites to phonolites (Peccerillo, 2017). The presence of intrusive calciocarbonatite ejecta (sövite), carbonatitic tephra in the pyroclastic products and carbonatite lava flows, witness the role of carbonatite magmatism beneath Mt. Vulture area (D'Orazio et al., 2007; Rosatelli et al., 2000; Stoppa & Principe, 1997), although the primary origin of the carbonate fraction is yet to be univocally accepted (D'Orazio et al., 2007, 2008; Stoppa et al., 2008).

The volcanic units of Mt. Vulture are divided into two Super-Synthems and five Synthems (Giannandrea et al., 2006). The Monticchio Lakes Synthem (MLS) represents the most recent activity of Vulture volcano and includes five Sub-Synthems, among which only Lago Piccolo is currently dated ( $132 \pm 12$  ka, Brocchini et al., 1994). Apparently, only three (Casa Rossa, Lago Piccolo and Serra di Braida) of the five Sub-Synthems of the MLS are characterised by the presence of abundant lapilli, ultramafic mantle xenoliths and mafic xenocrysts, described in depth for their petrographic and geochemical characterization (Downes et al., 2002; Jones et al., 2000; Rosatelli et al., 2007; Stoppa & Principe, 1997). They consist essentially of unaltered spinel-lherzolite, harzburgites, dunites, wehrlite and clinopyroxenites (Downes et al., 2002; Jones et al., 2000). Geothermobarometric studies (En-Sp and Di-Sp thermo-barometers) constrained pressures and temperatures in the range of 1.4-2.2 GPa and 1050-1150 °C respectively (Jones et al., 2000).

### **Petrography and Mineral Chemistry.**

The ultramafic cores of studied pelletal lapilli consist essentially of olivine and clinopyroxene phenocrysts with very rare orthopyroxene (wherlites), while few samples are characterised only by olivine megacrysts (dunites).

Olivine from the ultramafic cores of pelletal lapilli usually shows irregular elongated shape with curvilinear boundaries and also undulose extinction and intracrystalline deformation structures (see Figure 2 in the main text). Inclusions of spinel in olivine phenocrysts are also present. Clinopyroxene occurs as a distinctive emerald green coloured Cr-diopside and it occurs in all of the samples subhedral/anhedral with strongly curvilinear boundaries, apparently with no deformation structures.

Cr<sub>2</sub>O<sub>3</sub> content of olivine from the ultramafic cores of pelletal lapilli and of loose olivine xenocrysts varies in a very narrow range from 0.02 to 0.04 wt.% (Table S1).

SiO<sub>2</sub> and CaO content of clinopyroxene from the ultramafic core of pelletal lapilli ranges from 51.7 to 53.1 wt.% and from 22.2 to 22.9 wt.% respectively, while SiO<sub>2</sub> and CaO content in loose clinopyroxene xenocrysts ranges from 52.2 to 54.6 wt.% and from 20.1 to 22.7 wt.% respectively. The Mg# values are uniformly high, and they range from 0.90 to 0.92 (in ultramafic cores) and from 0.89 to 0.91 (in loose xenocrysts). TiO<sub>2</sub> and Al<sub>2</sub>O<sub>3</sub> content is low and ranges from 0.15 to 0.5 wt.% (in both ultramafic cores and loose xenocrysts) and from 3.6 to 4 wt.% (in ultramafic cores) and 2 to 5.5 wt.% (in loose xenocrysts), respectively (Table S2). The rim of ultramafic core of pelletal lapilli is composed of fine-grained micro-phenocrysts of h auyne, with xenocrystic debris of olivine and clinopyroxene (Figure S1).

Literature data refer of some crystal chemical and geochemical patterns in clinopyroxene such as the Ca/Al ratio, <sup>87</sup>Sr/<sup>86</sup>Sr ratio and also Mg#, as possible tracers of carbonatite mantle metasomatism (Zong & Liu, 2018). If plotted in Ca/Al vs Mg# and <sup>87</sup>Sr/<sup>86</sup>Sr vs Ca/Al diagrams, clinopyroxenes present as loose xenocrysts and in the Mt. Vulture xenoliths fall into the mantle-related carbonate metasomatism field (Figure S2). Indeed, clinopyroxenes from Mt. Vulture show restricted range of every ratio ( $5 \leq \text{Ca/Al} \leq 14$ ;  $0.88 \leq \text{Mg\#} \leq 0.91$ ;  $0.70424 \leq ^{87}\text{Sr}/^{86}\text{Sr} \leq 0.70585$ ) (data from Downes et al., 2002; Jones et al., 2000), in accordance with type 2 mantle-related carbonate metasomatism described by Zong and Liu (2018).

### **Fluid Inclusions.**

We analysed 171 fluid inclusions in loose xenocrysts of olivine, 107 in clinopyroxene (Cr-diopside), and 184 fluid inclusions in the ultramafic cores of studied lapilli (68 in olivine and 116 Cr-diopside) (Table S3), all being <10 µm in size and most of them in the range of 1-5 µm.

In loose xenocrysts, secondary fluid inclusions (distinguished on the basis of their textural characteristics and distribution within the crystals) are more abundant than primary fluid inclusions and tend to be smaller than the primary ones. On the contrary, in olivine and Cr-diopside in the ultramafic cores of pelletal lapilli, early stage fluid inclusions are more abundant than late stage fluid inclusions.

Trapping pressures and densities were estimated at the trapping temperature of 1100 °C, an intermediate temperature value of the temperature range (1050-1150 °C) previously calculated by Jones et al. (2000) with En-Sp and Di-Sp thermo-barometers. Finally, in order to convert barometric data into depths, we made some assumptions on crustal density of along the inferred magma pathway, using the stratigraphy presented in the CROP-4 deep seismic profile beneath the Mt. Vulture area (Scrocca et al., 2007). Considering (i) the average value of 2600 kg/m<sup>3</sup> of the shallow crust lithologies, (ii) an average value of 3300 kg/m<sup>3</sup> of the shallow mantle lithologies, and (iii) the probable presence of a mafic body beneath Mt. Vulture (Improta et al., 2014 and references therein), a single representative average value of 3000 kg/m<sup>3</sup> was considered.

## Analytical Methods

Mineral composition of analysed samples was determined by a CAMECA SX100 electron microprobe at Observatoire des Sciences de l'Univers (UPMC-INSU) (Paris, France), operating at 15 kV accelerating voltage and a 20nA beam current.

Fluid Inclusions were studied in doubly-polished wafers and single mineral grains by a Linkam THMSG 600 microscopic heating/cooling stage, at the Instituto de Vulcanologia e Avaliação de Riscos (IVAR) (Ponta Delgada, Portugal). Loose xenocrysts samples of olivine and clinopyroxene were embedded in epoxy resin and doubly polished until a thickness of 100-80  $\mu\text{m}$ . The stage was cooled with liquid nitrogen and calibrated using a single standard crystal of quartz with pure  $\text{H}_2\text{O}$  and  $\text{CO}_2$  inclusions. Cooling and heating rates varied during the analysis. Indeed, in order to minimize the effect of metastable transformations during cooling, very common in fluid inclusions, melting and homogenization temperatures were determined during heating at the minimum rate (1  $^\circ\text{C}/\text{min}$ ). For  $\text{CO}_2$ -rich inclusions ( $\text{H}_2\text{O}:\text{CO}_2$  ratio = 1:10) densities were firstly calculated on the basis of the equation provided in Sterner and Bodnar (1991) and finally corrected according to Hansteen and Klügel (2008), while isochores trajectories/curves were calculated using the software "Fluids" (Bakker, 2003).

## Geometric Parameters of Pelletal Lapilli.

In order to calculate all aspect ratio-related parameters of pelletal lapilli (i.e. major and minor axis, perimeter, cross-sectional area of rim and core and circularity values), individual samples were selected, digitised and processed in the image-analysis software package ImageJ, following the method of Gernon et al. (2012). The main geometric measurements of pelletal lapilli are reported in Table S4. The minimum axis of the entire pelletal lapilli sample data set range from 6.4 to 14 mm, while the maximum axis ranges from 6.9 to 16.1 mm. As regards the ultramafic cores of lapilli, the minimum axis ranges from 2.5 to 8.8 mm and the maximum axis ranges from 4.8 to 10 mm. The calculated cross-sectional areas of rims of pelletal lapilli show a good correlation with cross-sectional areas of cores (Figure S3), with a correlation coefficient  $r = 0.84$ . The circularity (defined as  $4\pi \times \text{area}/\text{perimeter}^2$ ) varies from 0.4 to 1.0 (i.e. 1.0 indicates a perfect circle), although the percentage frequency distribution shows that the most frequent value is 0.8 (Figure S3).

Pelletal lapilli associated with diatreme-maar systems present similar physical and geometrical characteristics to specific particles formed during an industrial process known as fluidised spray granulation process, widely used in industrial engineering and applied in geological contexts in some explosive eruptions (e.g., Gernon et al., 2012). The observed geometrical characteristics of Mt. Vulture pelletal lapilli (see Table S4) are similar to those of southern African ones associated with volcanoclastic kimberlite of Venetia and Letšeng (Gernon et al., 2012). Indeed, considering the evaluation of the aspect ratio and internal structure of both pelletal lapilli occurrences, they show moderate to strong positive correlation between the cross-sectional areas of rims and cores, with high circularity values (Figure S3), suggesting a uniform process of coating.

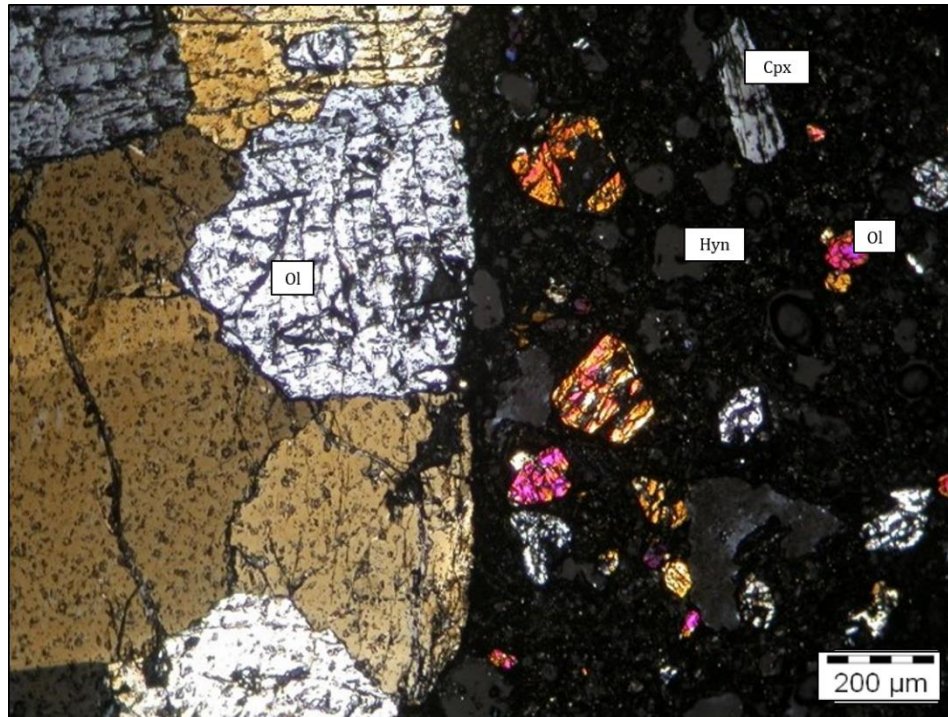


**Figure S1.** Crossed polars microphotograph showing the olivine micro-phenocrysts of the wehrlitic core of pelletal lapilli (on the left) and the rim of pelletal lapilli composed of fine-

grained micro-phenocrysts of h auyne and xenocrystic debris of olivine and clinopyroxene (on the right), Monticchio Lake Synthem, Mt. Vulture volcano.

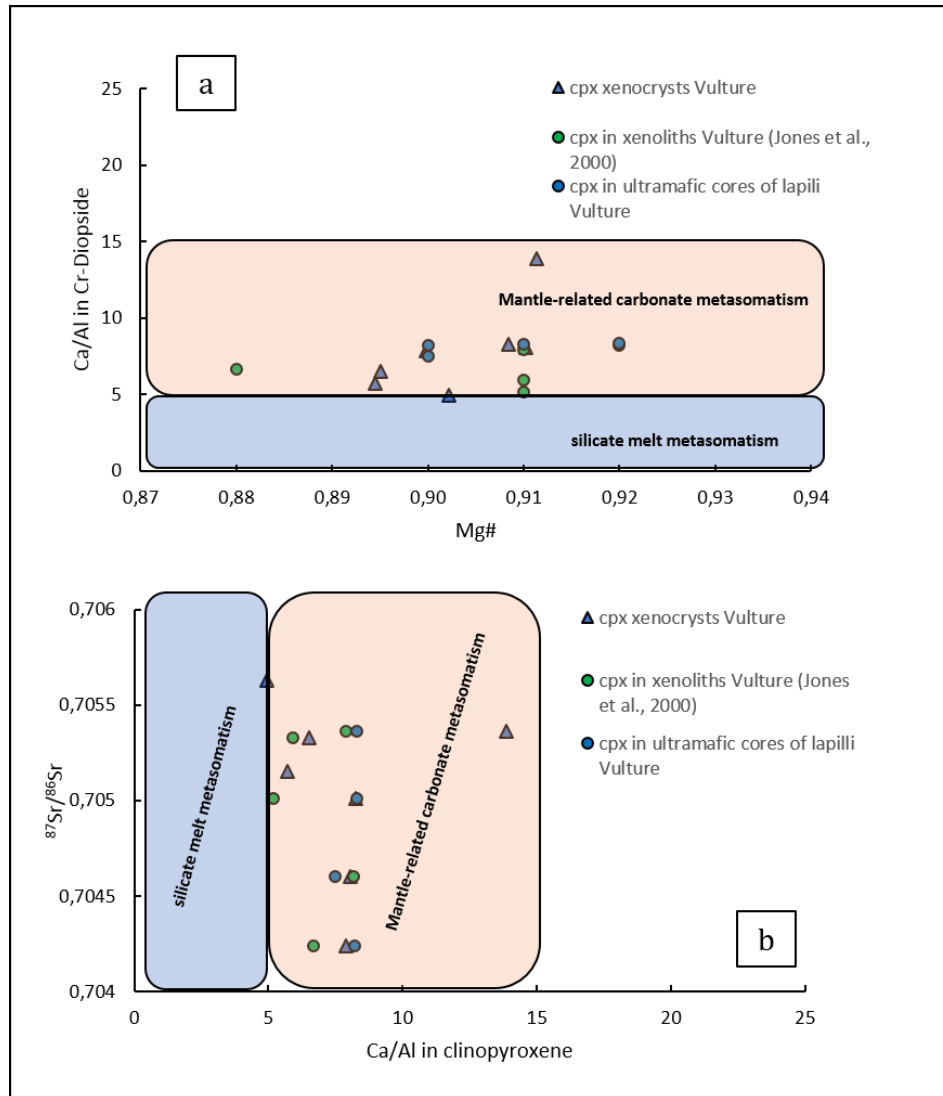


**Figure S2.** Ca/Al ratio vs. a) Mg# and b)  $^{87}\text{Sr}/^{86}\text{Sr}$  ratio of clinopyroxene from Mt. Vulture. Sr isotopic ratios are from Downes et al. (2002). Fields of carbonate vs. silicate melts metasomatism are taken from Zong and Liu (2018).

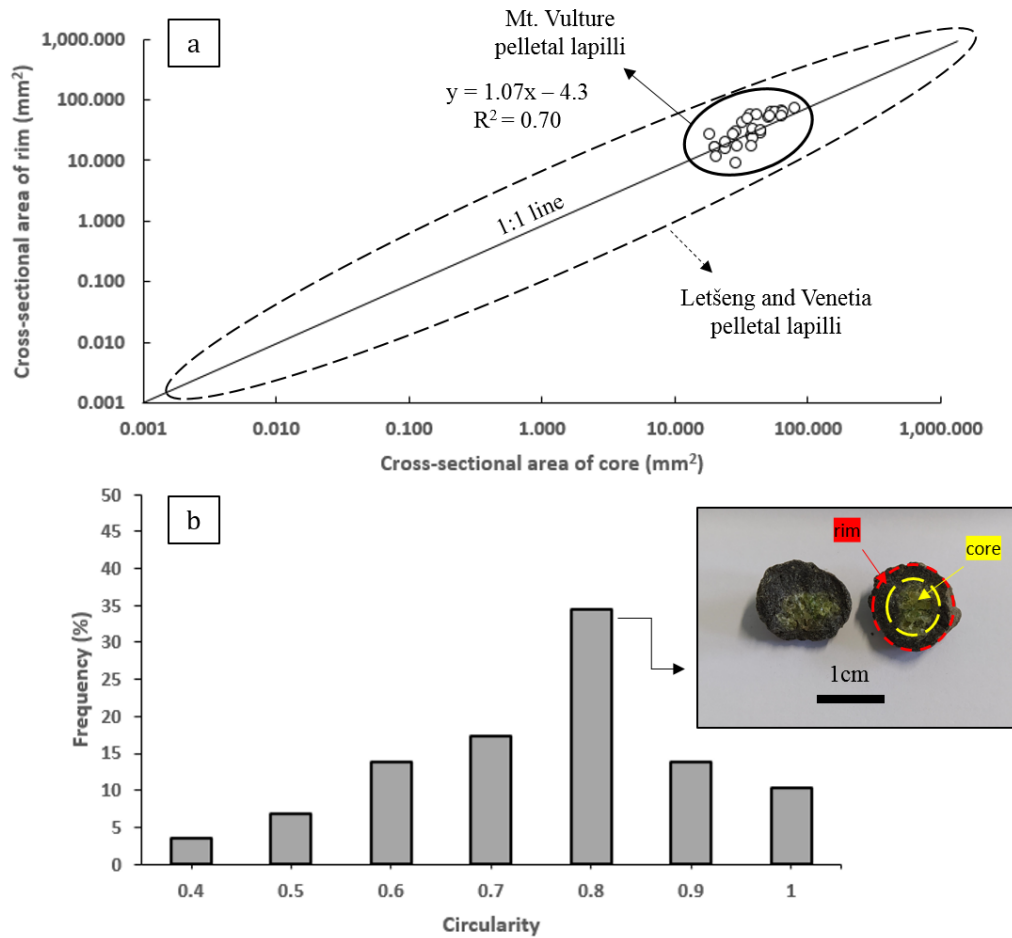


**Figure S3.** Diagrams of the main geometric characteristics of pelletal lapilli from Mt. Vulture. a) Cross-sectional area of core vs. cross-sectional area of rim (data of pelletal lapilli from Letšeng and Venetia are also plotted for comparison; Gernon et al., 2012). b) Histograms showing circularity values of pelletal lapilli.

**Table S1.** Minerochemical composition of olivine from the core of pelletal lapilli and loose olivine xenocrysts from Vulture volcano, Monticchio Lakes Synthem.

| Sample                         | ol-lap1 | ol-lap2 | ol-lap3 | ol-lap4 | ol-lap5 | ol-lap6 | ol-lap7 |
|--------------------------------|---------|---------|---------|---------|---------|---------|---------|
|                                | core    |
| SiO <sub>2</sub> (wt. %)       | 41.73   | 41.70   | 41.97   | 42.04   | 40.76   | 40.66   | 40.22   |
| FeO <sub>tot</sub>             | 8.97    | 9.15    | 9.02    | 8.97    | 9.03    | 10.07   | 9.00    |
| MnO                            | 0.14    | 0.14    | 0.14    | 0.14    | 0.13    | 0.16    | 0.14    |
| MgO                            | 49.62   | 49.79   | 49.66   | 49.71   | 50.09   | 50.80   | 51.48   |
| CaO                            | 0.09    | 0.09    | 0.08    | 0.09    | 0.09    | 0.10    | 0.09    |
| Cr <sub>2</sub> O <sub>3</sub> | 0.03    | 0.03    | 0.03    | 0.03    | 0.03    | 0.03    | 0.03    |

|      |        |        |        |        |        |        |        |
|------|--------|--------|--------|--------|--------|--------|--------|
| NiO  | 0.38   | 0.37   | 0.38   | 0.37   | 0.39   | 0.35   | 0.37   |
| Tot. | 100.95 | 101.27 | 101.28 | 101.35 | 100.52 | 102.16 | 101.33 |
| Mg#  | 0.91   | 0.91   | 0.91   | 0.91   | 0.91   | 0.90   | 0.91   |
| Fo   | 90.79  | 90.65  | 90.75  | 90.81  | 90.82  | 90.00  | 91.07  |
| Fa   | 9.21   | 9.35   | 9.25   | 9.19   | 9.18   | 10.00  | 8.93   |

Notes: Mg# = (Mg/Mg + Fe). Each reported analysis is the mean of three spots and core-rim analyses do not show significant zonation.

**Table S1.** Cont.

| <b>Sample</b>                  | ol-xeno1  | ol-xeno2  | ol-xeno3  | ol-xeno4  | ol-xeno5  | ol-xeno6  | ol-xeno7  |
|--------------------------------|-----------|-----------|-----------|-----------|-----------|-----------|-----------|
|                                | xenocryst |
| SiO <sub>2</sub> (wt. %)       | 40.50     | 39.65     | 40.56     | 41.50     | 40.09     | 41.67     | 40.97     |
| FeO <sub>tot</sub>             | 9.36      | 10.35     | 8.11      | 9.66      | 9.06      | 8.49      | 10.11     |
| MnO                            | 0.14      | 0.15      | 0.11      | 0.13      | 0.12      | 0.11      | 0.14      |
| MgO                            | 49.87     | 48.97     | 50.75     | 50.72     | 49.83     | 49.60     | 50.32     |
| CaO                            | 0.15      | 0.14      | 0.19      | 0.18      | 0.12      | 0.18      | 0.14      |
| Cr <sub>2</sub> O <sub>3</sub> | 0.03      | 0.02      | 0.04      | 0.02      | 0.04      | 0.03      | 0.02      |
| NiO                            | 0.38      | 0.37      | 0.41      | 0.37      | 0.40      | 0.39      | 0.37      |
| Tot.                           | 100.43    | 99.64     | 100.16    | 102.59    | 99.66     | 100.48    | 102.07    |
| Mg#                            | 0.90      | 0.89      | 0.92      | 0.90      | 0.91      | 0.91      | 0.90      |
| Fo                             | 90.48     | 89.40     | 91.78     | 90.35     | 90.75     | 91.24     | 89.87     |
| Fa                             | 9.52      | 10.60     | 8.22      | 9.65      | 9.25      | 8.76      | 10.13     |

Notes: Mg# = (Mg/Mg + Fe). Each reported analysis is the mean of three spots and core-rim analyses do not show significant zonation.

**Table S2.** Minerochemical composition of clinopyroxene from the core of pelletal lapilli and loose clinopyroxene xenocrysts from Vulture volcano, Monticchio Lakes Synthem.

| <b>Sample</b>                  | Cr-di lap1 | Cr-di lap2 | Cr-di lap3 | Cr-di lap4 |
|--------------------------------|------------|------------|------------|------------|
|                                | core       | core       | core       | core       |
| SiO <sub>2</sub> (wt. %)       | 52.3039    | 52.9848    | 53.1418    | 51.7559    |
| TiO <sub>2</sub>               | 0.33       | 0.40       | 0.15       | 0.48       |
| Al <sub>2</sub> O <sub>3</sub> | 3.63       | 3.72       | 3.68       | 4.02       |
| FeO                            | 2.78       | 2.59       | 3.13       | 3.40       |
| MnO                            | 0.00       | 0.00       | 0.00       | 0.00       |
| MgO                            | 16.20      | 16.55      | 16.40      | 16.44      |

|                                |       |        |        |        |
|--------------------------------|-------|--------|--------|--------|
| CaO                            | 22.29 | 22.90  | 22.40  | 22.24  |
| Na <sub>2</sub> O              | 0.62  | 0.56   | 0.52   | 0.49   |
| Cr <sub>2</sub> O <sub>3</sub> | 1.35  | 1.31   | 1.47   | 1.29   |
| Tot.                           | 99.50 | 101.01 | 100.89 | 100.12 |
| Mg#                            | 0.91  | 0.92   | 0.90   | 0.90   |
| Wo                             | 47.42 | 47.76  | 46.99  | 46.57  |
| En                             | 47.96 | 48.02  | 47.88  | 47.88  |
| Fs                             | 4.62  | 4.22   | 5.13   | 5.55   |

Notes: Mg# = (Mg/Mg + Fe). Each reported analysis is the mean of three spots and core-rim analyses do not show significant zonation.

**Table S2.** Cont.

| <b>Sample</b>                  | Cr-di1    | Cr-di2    | Cr-di3    | Cr-di4    | Cr-di5    | Cr-di6    | Cr-di7    |
|--------------------------------|-----------|-----------|-----------|-----------|-----------|-----------|-----------|
|                                | xenocryst |
| SiO <sub>2</sub> (wt. %)       | 54.56     | 53.09     | 52.91     | 52.81     | 53.13     | 52.46     | 52.19     |
| TiO <sub>2</sub>               | 0.16      | 0.31      | 0.37      | 0.38      | 0.43      | 0.14      | 0.48      |
| Al <sub>2</sub> O <sub>3</sub> | 2.09      | 3.67      | 3.84      | 3.80      | 4.55      | 5.48      | 5.19      |
| FeO                            | 3.02      | 2.90      | 3.20      | 2.91      | 3.33      | 3.20      | 3.42      |
| MnO                            | 0.00      | 0.00      | 0.00      | 0.00      | 0.00      | 0.00      | 0.00      |
| MgO                            | 17.42     | 16.12     | 16.12     | 16.52     | 15.91     | 16.55     | 16.25     |
| CaO                            | 21.43     | 22.41     | 22.38     | 22.71     | 21.91     | 20.15     | 21.98     |
| Na <sub>2</sub> O              | 0.73      | 0.64      | 0.71      | 0.61      | 0.75      | 1.10      | 0.79      |
| Cr <sub>2</sub> O <sub>3</sub> | 1.15      | 1.28      | 0.92      | 0.93      | 0.42      | 1.25      | 0.86      |
| Tot.                           | 100.55    | 100.42    | 100.45    | 100.67    | 100.42    | 100.33    | 101.16    |
| Mg#                            | 0.91      | 0.91      | 0.90      | 0.91      | 0.90      | 0.90      | 0.89      |
| Wo                             | 44.62     | 47.58     | 47.31     | 47.34     | 46.97     | 44.12     | 46.51     |
| En                             | 50.47     | 47.62     | 47.42     | 47.93     | 47.47     | 50.42     | 47.84     |
| Fs                             | 4.91      | 4.80      | 5.28      | 4.73      | 5.56      | 5.47      | 5.64      |

Notes: Mg# = (Mg/Mg + Fe). Each reported analysis is the mean of three spots and core-rim analyses do not show significant zonation.

**Table S3.** Micro-thermometric data of studied samples.

| <b>Sample</b> | <b>Mineral analysed</b> | <b>N° measures</b> | <b>Th (°C)</b>              | <b>ρ (g/cm<sup>3</sup>)</b> | <b>ρ (g/cm<sup>3</sup>)<sub>corrected</sub></b> |
|---------------|-------------------------|--------------------|-----------------------------|-----------------------------|---|
| Ol-I          | olivine (5)             | 46                 | Th <sub>L</sub> 11.5 – 30.2 | 0.58 – 0.85                 | 0.61 – 0.89                                     |
| Ol-II         | olivine (1)             | 12                 | Th <sub>L</sub> 13.0 – 20.9 | 0.76 – 0.84                 | 0.80 – 0.88                                     |

|           |                   |     |                               |             |             |
|-----------|-------------------|-----|-------------------------------|-------------|-------------|
| OI-III    | olivine (2)       | 113 | Th <sub>L</sub> 23.3 – 30.9   | 0.52 – 0.73 | 0.54 – 0.77 |
| Cr-cpx I  | clinopyroxene (2) | 77  | Th <sub>L</sub> 2.7 – 13.2    | 0.84 – 0.91 | 0.88 – 0.95 |
| Cr-cpx II | clinopyroxene (1) | 30  | Th <sub>L</sub> -20.0 – -15.1 | 1.01 – 1.03 | 1.05 – 1.08 |
| LAP-1     | olivine (1)       | 40  | Th <sub>L</sub> -27.7 – -23.4 | 1.05 – 1.07 | 1.10 – 1.11 |
|           | clinopyroxene (2) | 36  | Th <sub>L</sub> -27.3 – -8.5  | 0.98 – 1.06 | 1.02 – 1.11 |
| LAP-2     | olivine (1)       | 28  | Th <sub>L</sub> -9.0 – 30.3   | 0.58 – 0.98 | 0.60 – 1.02 |
|           | clinopyroxene (1) | 80  | Th <sub>L</sub> -13.5 – -11.5 | 0.99 – 1.00 | 1.04 – 1.05 |

Notes: in brackets the number of analysed minerals; Th= homogenization temperature; ρ = density

**Table S4.** Calculated geometric parameters of studied pelletal lapilli from Vulture volcano, Monticchio Lakes Synthem.

| <b>Sample</b> | <b>ax<sub>min</sub> (mm)</b> | <b>ax<sub>max</sub></b> | <b>ax core<sub>min</sub></b> | <b>ax core<sub>max</sub></b> | <b>P (mm)</b> | <b>P core</b> | <b>A (mm<sup>2</sup>)</b> | <b>A core</b> | <b>A rim</b> | <b>circularity</b> |
|---------------|------------------------------|-------------------------|------------------------------|------------------------------|---------------|---------------|---------------------------|---------------|--------------|--------------------|
| LAP-1W        | 14.0                         | 15.0                    | 7.5                          | 10.0                         | 47.1          | 31.4          | 153.9                     | 78.5          | 75.4         | 0.9                |
| LAP-2W        | 13.0                         | 15.8                    | 6.7                          | 9.0                          | 49.6          | 28.3          | 132.7                     | 63.6          | 69.1         | 0.7                |
| LAP-3W        | 11.4                         | 14.7                    | 7.9                          | 8.0                          | 46.2          | 25.1          | 102.0                     | 50.2          | 51.8         | 0.6                |
| LAP-4W        | 8.7                          | 9.7                     | 3.7                          | 6.0                          | 30.5          | 18.8          | 59.4                      | 28.3          | 31.2         | 0.8                |
| LAP-5W        | 7.1                          | 8.2                     | 4.1                          | 5.5                          | 25.7          | 17.3          | 39.6                      | 23.7          | 15.8         | 0.7                |
| LAP-6W        | 9.7                          | 11.9                    | 7.0                          | 7.5                          | 37.4          | 23.6          | 73.9                      | 44.2          | 29.7         | 0.7                |
| LAP-7W        | 9.8                          | 12.5                    | 3.8                          | 6.4                          | 39.3          | 20.1          | 75.4                      | 32.2          | 43.2         | 0.6                |
| LAP-8W        | 12.2                         | 14.9                    | 4.0                          | 8.2                          | 46.8          | 25.7          | 116.8                     | 52.8          | 64.1         | 0.7                |
| LAP-9W        | 12.5                         | 14.0                    | 6.0                          | 8.5                          | 44.0          | 26.7          | 122.7                     | 56.7          | 65.9         | 0.8                |
| LAP-10W       | 11.0                         | 16.1                    | 2.5                          | 6.8                          | 50.6          | 21.4          | 95.0                      | 36.3          | 58.7         | 0.5                |
| LAP-11ol      | 9.3                          | 10.3                    | 6.6                          | 7.0                          | 32.3          | 22.0          | 67.9                      | 38.5          | 29.4         | 0.8                |
| LAP-12ol      | 12.8                         | 14.5                    | 8.8                          | 9.1                          | 45.5          | 28.6          | 128.6                     | 65.0          | 63.6         | 0.8                |
| LAP-13D       | 12.3                         | 12.4                    | 5.0                          | 9.0                          | 38.9          | 28.3          | 118.8                     | 63.6          | 55.2         | 1.0                |
| LAP-14ol      | 9.0                          | 10.6                    | 6.5                          | 6.9                          | 33.3          | 21.7          | 63.6                      | 37.4          | 26.2         | 0.7                |
| LAP-15D       | 11.3                         | 11.4                    | 5.9                          | 7.2                          | 35.8          | 22.6          | 100.2                     | 40.7          | 59.5         | 1.0                |
| LAP-16ol      | 8.9                          | 10.0                    | 4.1                          | 7.0                          | 31.4          | 22.0          | 62.2                      | 38.5          | 23.7         | 0.8                |
| LAP-17W       | 9.6                          | 9.7                     | 6.8                          | 7.0                          | 30.5          | 22.0          | 72.3                      | 38.5          | 33.9         | 1.0                |
| LAP-18W       | 6.8                          | 7.5                     | 3.9                          | 5.0                          | 23.6          | 15.7          | 36.3                      | 19.6          | 16.7         | 0.8                |
| LAP-19W       | 7.7                          | 8.8                     | 5.8                          | 6.1                          | 27.6          | 19.2          | 46.5                      | 29.2          | 17.3         | 0.8                |
| LAP-20D       | 6.9                          | 10.5                    | 5.7                          | 6.0                          | 33.0          | 18.8          | 37.4                      | 28.3          | 9.1          | 0.4                |
| LAP-21W       | 6.8                          | 7.3                     | 4.5                          | 5.0                          | 22.9          | 15.7          | 36.3                      | 19.6          | 16.7         | 0.9                |
| LAP-22D       | 7.6                          | 10.0                    | 4.7                          | 4.8                          | 31.4          | 15.1          | 45.3                      | 18.1          | 27.3         | 0.6                |
| LAP-23D       | 8.4                          | 11.0                    | 4.6                          | 5.9                          | 34.5          | 18.5          | 55.4                      | 27.3          | 28.1         | 0.6                |
| LAP-24W       | 6.4                          | 6.9                     | 5.0                          | 5.1                          | 21.7          | 16.0          | 32.2                      | 20.4          | 11.7         | 0.9                |
| LAP-25W       | 8.4                          | 9.2                     | 6.8                          | 6.9                          | 28.9          | 21.7          | 55.4                      | 37.4          | 18.0         | 0.8                |
| LAP-26W       | 9.9                          | 10.7                    | 6.8                          | 7.5                          | 33.6          | 23.6          | 76.9                      | 44.2          | 32.8         | 0.9                |
| LAP-27D       | 11.7                         | 12.8                    | 7.0                          | 8.1                          | 40.2          | 25.4          | 107.5                     | 51.5          | 56.0         | 0.8                |
| LAP-28W       | 7.5                          | 10.6                    | 5.3                          | 5.5                          | 33.3          | 17.3          | 44.2                      | 23.7          | 20.4         | 0.5                |
| LAP-29W       | 10.4                         | 11.3                    | 5.5                          | 6.7                          | 35.5          | 21.0          | 84.9                      | 35.2          | 49.7         | 0.8                |

Notes: W = wehrlite; D = dunite; ol = olivine; ax = axis; P = perimeter; A = area.

## References.

- Bakker, R. J. (2003). Package FLUIDS 1. Computer programs for analysis of fluid inclusion data and for modelling bulk fluid properties. *Chemical Geology*, 194(1–3), 3–23. [https://doi.org/10.1016/S0009-2541\(02\)00268-1](https://doi.org/10.1016/S0009-2541(02)00268-1)
- Brocchini, D., La Volpe, L., Laurenzi, M. A., & Principe, C. (1994). Storia evolutiva del Monte Vulture. *Plinius*, 12, 22–25.
- D’Orazio, M., Innocenti, F., Tonarini, S., & Doglioni, C. (2007). Carbonatites in a subduction system: The Pleistocene alvikites from Mt. Vulture (southern Italy). *Lithos*, 98(1–4), 313–334. <https://doi.org/10.1016/j.lithos.2007.05.004>
- D’Orazio, M., Innocenti, F., Tonarini, S., & Doglioni, C. (2008). Reply to the discussion of: “Carbonatites in a subduction system: The Pleistocene alvikites from Mt. Vulture (Southern Italy)” by M. D’Orazio, F. Innocenti, S. Tonarini and C. Doglioni (Lithos 98, 313–334) by F. Stoppa, C. Principe and P. Giannandrea. *Lithos*, 103(3–4), 557–561. <https://doi.org/10.1016/j.lithos.2007.10.010>
- Downes, H., Kostoula, T., Jones, A. P., Beard, A. D., Thirlwall, M. F., & Bodinier, J. L. (2002). Geochemistry and Sr-Nd isotopic compositions of mantle xenoliths from the Monte Vulture carbonatite-melilitite volcano, central southern Italy. *Contributions to Mineralogy and Petrology*, 144(1), 78–92. <https://doi.org/10.1007/s00410-002-0383-4>
- Gernon, T. M., Brown, R. J., Tait, M. A., & Hincks, T. K. (2012). The origin of pelletal lapilli in explosive kimberlite eruptions. *Nature Communications*, 3(May), 832–837. <https://doi.org/10.1038/ncomms1842>
- Giannandrea, P., La Volpe, L., Principe, C., & Schiattarella, M. (2006). Unità stratigrafiche a limiti inconformi e storia evolutiva del vulcano medio-pleistocenico di Monte Vulture (Appennino meridionale, Italia). *Bollettino Della Societa Geologica Italiana*, 125(1), 67–92.
- Hansteen, T. H., & Klügel, A. (2008). Fluid inclusion thermobarometry as a tracer for magmatic processes. *Reviews in Mineralogy and Geochemistry*, 69(Roedder 1984), 143–177. <https://doi.org/10.2138/rmg.2008.69.5>
- Improta, L., De Gori, P., & Chiarabba, C. (2014). New insights into crustal structure, Cenozoic magmatism, CO<sub>2</sub> degassing, and seismogenesis in the southern Apennines and Irpinia region from local earthquake tomography. *Journal of Geophysical Research: Solid Earth*, 119(11), 8283–8311. <https://doi.org/10.1002/2013JB010890>
- Jones, A. P., Kostoula, T., Stoppa, F., & Woolley, A. R. (2000). Petrography and mineral chemistry of mantle xenoliths in a carbonate-rich melilititic tuff from Mt. Vulture volcano, southern Italy. *Mineralogical Magazine*, 64(4), 593–613.

<https://doi.org/10.1180/002646100549634>

- Kelemework, Y., Milano, M., La Manna, M., de Alteriis, G., Iorio, M., & Fedi, M. (2021). Crustal structure in the Campanian region (Southern Apennines, Italy) from potential field modelling. *Scientific Reports*, *11*(1), 1–18. <https://doi.org/10.1038/s41598-021-93945-8>
- Peccerillo, A. (2017). The Apulian Province (Mount Vulture). *Advances in Volcanology*, 203–216. [https://doi.org/10.1007/978-3-319-42491-0\\_8](https://doi.org/10.1007/978-3-319-42491-0_8)
- Rosatelli, G., Stoppa, F., & Jones, A. P. (2000). Intrusive calcite-carbonatite occurrence from Mt. Vulture volcano, southern Italy. *Mineralogical Magazine*, *64*(4), 615–624. <https://doi.org/10.1180/002646100549643>
- Rosatelli, G., Wall, F., & Stoppa, F. (2007). Calcio-carbonatite melts and metasomatism in the mantle beneath Mt. Vulture (Southern Italy). *Lithos*, *99*(3–4), 229–248. <https://doi.org/10.1016/j.lithos.2007.05.011>
- Scrocca, D., Sciamanna, S., Di Luzio, E., Tozi, M., Nicolai, C., & Gambini, R. (2007). Structural setting along the CROP-04 deep seismic profile (Southern Apennines - Italy). *Bollettino Della Societa Geologica Italiana, Supplemento*, *7*(February 2007), 283–296.
- Sterner, S. M., & Bodnar, R. J. (1991). Synthetic fluid inclusions. X: Experimental determination of P-V-T-X properties in the CO<sub>2</sub>-H<sub>2</sub>O system to 6 kb and 700 °C. *American Journal of Science*, *291*, 1–54. <https://doi.org/https://doi.org/10.2475/ajs.291.1.1>
- Stoppa, F., Principe, C., & Giannandrea, P. (2008). Comments on: Carbonatites in a subduction system: The Pleistocene alvikites from Mt. Vulture (southern Italy) by d’Orazio et al., (2007). *Lithos*, *103*(3–4), 550–556. <https://doi.org/10.1016/j.lithos.2007.10.012>
- Stoppa, F., & Principe, C. (1997). Eruption style and petrology of a new carbonatitic suite from the Mt. Vulture Southern Italy /: The Monticchio Lakes Formation. *Journal of Volcanology and Geothermal Research*, *78*(3–4), 251–265. [https://doi.org/10.1016/S0377-0273\(97\)00004-8](https://doi.org/10.1016/S0377-0273(97)00004-8)
- Villa, I. M., & Buettner, A. (2009). Chronostratigraphy of Monte Vulture volcano (southern Italy): Secondary mineral microtextures and <sup>39</sup>Ar-<sup>40</sup>Ar systematics. *Bulletin of Volcanology*, *71*(10), 1195–1208. <https://doi.org/10.1007/s00445-009-0294-6>
- Zong, K., & Liu, Y. (2018). Carbonate metasomatism in the lithospheric mantle: Implications for cratonic destruction in North China. *Science China Earth Sciences*, *61*(6), 711–729. <https://doi.org/10.1007/s11430-017-9185-2>